INL/CON-16-38140
PREPRINT

Numerical Study of Critical Role of Rock Heterogeneity in Hydraulic Fracture Propagation

50th U.S. Rock Mechanics/Geomechanics Symposium

J. Zhou and H. Huang
(Idaho National Laboratory)

M. Deo
(University of Utah)

March 2016

The INL is a
U.S. Department of Energy
National Laboratory
operated by
Battelle Energy Alliance

Numerical Study of Critical Role of Rock Heterogeneity in Hydraulic Fracture Propagation

Zhou, J.
Idaho National Laboratory, Idaho Falls, Idaho, USA
Huang, H
Idaho National Laboratory, Idaho Falls, Idaho, USA
Deo, M.
Department of Chemical Engineering, the University of Utah, Salt Lake City, Utah, USA

ABSTRACT: Log and seismic data indicate that most shale formations have strong heterogeneity. Conventional analytical and semi-analytical fracture models are not enough to simulate the complex fracture propagation in these highly heterogeneous formations. Without considering the intrinsic heterogeneity, predicted morphology of hydraulic fracture may be biased and misleading in optimizing the completion strategy. In this paper, a fully coupling fluid flow and geomechanics hydraulic fracture simulator based on dual-lattice Discrete Element Method (DEM) is used to predict the hydraulic fracture propagation in heterogeneous reservoir. The heterogeneity of rock is simulated by assigning different material force constant and critical strain to different particles and is adjusted by conditioning to the measured data and observed geological features. Based on proposed model, the effects of heterogeneity at different scale on micromechanical behavior and induced macroscopic fractures are examined. From the numerical results, the microcrack will be more inclined to form at the grain weaker interface. The conventional simulator with homogeneous assumption is not applicable for highly heterogeneous shale formation.

1. INTRODUCTION

Hydraulic fracturing is a well-stimulation technique, which creates fractures in rock formations through the injection of hydraulically pressurized fluid. Since the 1950s, about 70% of gas wells and 50% of oil wells have been hydraulically fractured [1]. Wide and successful applications of horizontal wells and hydraulic fracturing are the key reasons leading to the exponentially growing of tight oil and shale gas production. Therefore, understanding the hydraulic fracture propagation in complex unconventional reservoir plays a crucial role in optimizing the stimulation strategy and maximizing the created contacting surface.

However, there are several challenges in precisely predicting and controlling the induced fracture geometry [2]. One significant difficulty is that rock is a heterogeneous material containing many natural weaknesses, including pores, grain boundaries, and pre-existing fractures [3]. Microseismic monitoring, production data, log, and seismic data confirm that the reservoir formation has strong lateral heterogeneity, which is a key impact factor of rock's mechanical behaviors. During the hydraulic fracturing process, these pre-existing weaknesses can induce microcracks or microfractures, which can in turn change the flow capability of the rock [4], [5]. For example, the Bakken formation is a layered heterogeneous reservoir, which is separated into upper, middle, lower and three forks. And even in one layer, the rock mineralogy varies with depth and location. Thus, without considering the intrinsic heterogeneity, the predicted morphology of hydraulic fracture may be biased and misleading in guiding the horizontal well completion strategy.

The generated fracture morphology is not easily characterized through existing diagnostic methods or by conducting laboratory experiments. Development of a physical rigorous tool provides an added way for understanding the hydraulic fractures network under realistic conditions. Hydraulic fracturing models have evolved from two-dimensional models to three-dimensional models, from bi-wing planar fracture geometry to dendrite-type complex fracture networks. Traditional hydraulic fracturing simulators assumed single bi-wing planar fracture with a penny-shaped fracture geometry extending from the wellbore to the formation. Fracture initiation and propagation direction are obtained through the calculation of stress intensity factor and different criteria. Usually, the theory of linear elasticity is used to model the rock deformation, the fluid flow is simulated using lubrication theory, and the linear elastic fracture mechanics (LEFM) theory is adopted to

determine the fracture propagation [6], [7]. Two typical traditional models used to predict the hydraulic fracture geometry are the Khristianovich-Geertsma-DeKlerk (KGD) model [8], [9] and the Perkins-Kern-Nordgren (PKN) model [10], [11]. Both models assume the plane strain deformation (two-dimensional model) and calculate fracture width based on the analytical solution. Both KGD and PKN models have limitations in their application because they oversimplify the fracture propagation problems.

In order to account for the mechanical interactions and overcome the limitations of bi-wing fracture model, a variety of nonplanar hydraulic fracturing models have been proposed in recent years [12], [13]. One widely used method is the displacement discontinuity method (DDM), which is an indirect boundary element method developed by Crouch [14]. In the DDM method, when deformation at the fracture tip reaches the critical threshold, the fracture will move forward. The fracture propagation length and direction are obtained through the calculation of stress intensity factor at the fracture tip. Compared with other methods, the DDM reduces the dimensions of the problem by one through discretizing only the boundaries rather than whole domain [15]. Therefore, the DDM exhibits higher computational efficiency and more accuracy, which makes it very suitable for predicting fracture propagation in a large field-scale reservoir. However this model is not efficient in dealing with material heterogeneity and nonlinear material behaviors. Shin and Sharma [16] simulated multiple hydraulic fracture propagation using ABAQUS Standard finite element analysis software. The reservoir is modeled as a porous elastic medium, and pore pressure cohesive elements are inserted at each perforation cluster to model fracture propagation. The simulators based on the finite-element method utilized various remeshing strategies to explicitly simulate the crack propagation, which are inefficient and time consuming for transferring the information between different meshes. To avoid the remeshing issue and improve efficiency, the Extended Finite Element Method (XFEM) is proposed [17]. The XFEM allows fractures to propagate directly cross the element, independent of the mesh configuration. The XFEM is a promising technology in simulating fracture propagation because of its ability to deal with heterogeneous reservoir and complex boundary condition. However, the computational load of this method is too large to be applicable to large-scale problems.

In this paper, a new developed fully coupling fluid flow and geomechanics hydraulic fracture simulator based on dual-lattice discrete element method (DL-DEM) [18] is used to predict the hydraulic fracture propagation in heterogeneous reservoir. Based on proposed model, the effects of heterogeneity at different scales on micromechanical behavior and induced macroscopic fractures are examined.

2. METHODOLOGY

In the dual-lattice DEM model, illustrated by Figure 1, rock is represented by an assembly of randomly generated, non-uniform-sized circular rigid particles that may be connected by elastic beams (whether two particles are connected by a beam is determined by their relative distance). The mechanical behavior of the rock is mimicked by the movements of particles and the status of the connected beams. When a load is applied, the beam between two particles will sustain increasing force, which may lead to bond breakage and form microcracks. With continued application of the load, these microcracks may coalesce and become macroscopic features.

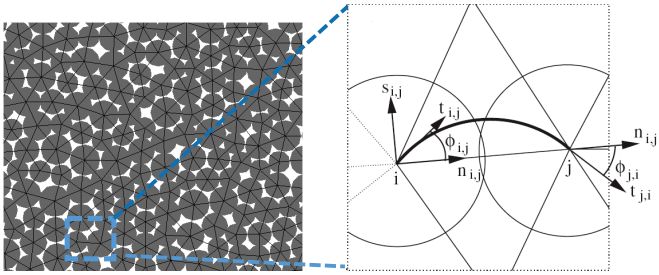

Fig. 1. Illustration of a 2-dimensional (2D) DEM model.

In order to fully couple geomechanics with flow, a conjugate flow lattice is added to the system to form a dual-lattice system. The DEM network is used to calculate the mechanical interaction between particles, and the conjugate flow lattice is used to explicitly simulate the fluid injection and calculate the pressure gradient. The concept of dual-lattice is shown in Figure 2. In this figure, the black lattice represents DEM lattice, and the red lattice is conjugate flow lattice.

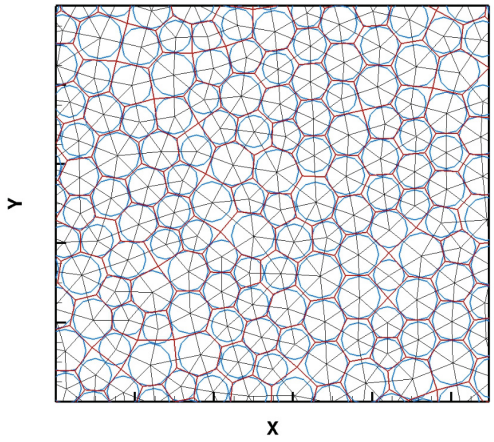

Fig. 2. The concept of dual lattice used in the simulator.

Unlike other DEM-based fracture simulators, such as PFC2D or PFC3D (Itasca, Inc) [19], [20], which mimic the dynamic process, the current simulator treats fracture

propagation as a quasi-static process wherein the particles keep moving until a stress equilibrium is achieved for each time step. Attaining equilibrium in each time step is an important assumption made in the algorithm employed. This assumption is reasonable, taking into consideration the fact that fluid leakoff and transport rate are much slower compared to force transmission and fracture propagation.

The forces of all stressed particles can be obtained by tracing the movements of individual particles and their relative distances. In a DEM model with confined volume, movements of particles will result from the propagation disturbance caused by the formation boundary, neighboring particles' motion, external applied forces, and body force [20]. The resultant displacements and rotations of all DEM particles are determined by both force magnitude and particle properties.

After considering all different mechanisms and the existence of beams, the displacement and rotation of each DEM particle may result from the combined effects from the following forces, leading to the formation of hydraulic fractures:

1. External force caused by the fluid injection and pressure gradient.
2. Beam force and moment from the beam-connected particles.
3. Viscous damping force.
4. The interaction with neighboring particles that do not have beam connection.
5. The interaction between particles and walls.

Figure 3 depicts the calculation steps used in the model. Since this method is quasi-static, the dynamic step of calculating particle velocity and acceleration is not required. Force-Displacement law is used to determine both the translational and rotational motion of each particle and the contact forces after particle displacement.

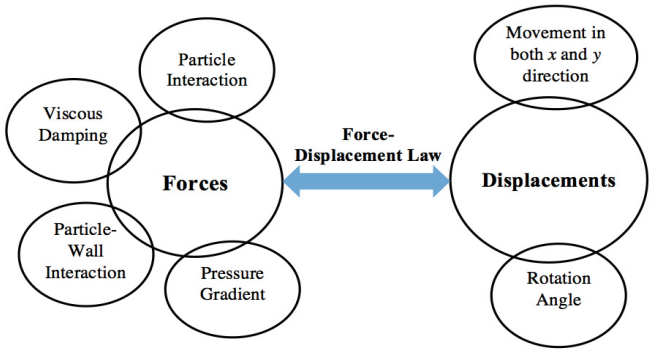

Fig. 3. The algorithm of quasistatic DL-DEM hydraulic fracture simulator.

As shown in Figure 1, the force vector, $\vec{F}_{i,j}$, contains normal and shear force components:

$$\vec{F}_{i,j} = F_{i,j}^{n}\vec{n}_{i,j} + F_{i,j}^{s}\vec{s}_{i,j} \tag{1}$$

where $F_{i,j}^{n}$ and $F_{i,j}^{s}$ are the normal and shear force. $\vec{n}_{i,j}$ and $\vec{s}_{i,j}$ are the unit vectors parallel and perpendicular to the center line connecting nodes *i* and *j*. $\vec{t}_{i,j}$ is the unit vector parallel to the tangent of the bent beam at node *i*. $F_{i,j}^{n}$ and $F_{i,j}^{s}$ can be calculated as:

$$\begin{cases} F_{i,j}^{n} = k_n\left(d_{i,j} - d_{i,j}^{0}\right) \\ F_{i,j}^{s} = k_s\dfrac{1}{2}\left(\phi_{i,j} + \phi_{j,i}\right) \end{cases} \tag{2}$$

Where $d_{i,j} = \left|\overline{(x,y)}_i - \overline{(x,y)}_j\right|$ is the distance between the centers of two DEM nodes (the centers of the corresponding particles), *i* and *j*, and $d_{i,j}^{0} = r_i + r_j$ is the initial equilibrium (stress free) distance, where r_i is the radius of the i^{th} particle. $\phi_{i,j}$ is the rotation angle in the local frame of the beam. k_n and k_s are the normal and shear force constants which are given by

$$\begin{cases} k_n = \dfrac{1}{2}\left(k_n^i + k_n^j\right) \\ k_s = \dfrac{1}{2}\left(k_s^i + k_s^j\right) \end{cases} \tag{3}$$

here k_n^i, k_n^j and k_s^i, k_s^j are the normal and shear force constant of particle *i* and *j* respectively. Since the DEM particles are generated and distributed randomly, k_n and k_s must be calibrated against the desired E_0 and ν. The detailed calibration process has been described in Huang and Mattson[21].

Without considering the forces caused by fluid flow and pressure accumulation, the force and moment exerted on a node *i* by a neighboring, connected node *j* are given by

$$\vec{F}_{i,j} = k_n\left(d_{i,j} - d_{i,j}^{0}\right)\vec{n}_{i,j} + k_s\frac{1}{2}\left(\phi_{i,j} + \phi_{j,i}\right)\vec{s}_{i,j} \tag{4}$$

$$\vec{M}_{i,j} = k_s d_{i,j}\left[\frac{\Phi}{12}\left(\phi_{i,j} - \phi_{j,i}\right) + \frac{1}{2}\left(\frac{2}{3}\phi_{i,j} + \frac{1}{3}\phi_{j,i}\right)\right] \tag{5}$$

where $\Phi = 12E_0 I/G_0 A d^2$, I is moment of inertia.

There are different criteria to evaluate the rock behavior such as stress-based failure criteria, strain-based failure criteria and energy typed failure criteria. Unlike the Displacement Discontinuity or analytical models, which obtain the fractures propagation length and direction by calculating the stress intensity factor, we utilize a more straightforward and quantitative criterion to simulate fracture growth – the von Mises failure criterion. If a beam satisfies the von Mises failure criterion

$$\left(\frac{\varepsilon}{\varepsilon_c}\right)^2 + \frac{\max\left(\left|\phi_{i,j}\right|,\left|\phi_{j,i}\right|\right)}{\phi_c} > 1 \qquad (6)$$

it will be irreversibly removed from the DEM network, giving rise to crack initiation and growth. Here ε is the longitudinal strain of the beam, and ε_c is the critical longitudinal tensile strain (the maximum tensile strain that the bond can sustain), and ϕ_c is the critical rotational angle above which the bond will break, even in the absence of tensile strain. Typical values for ε_c and ϕ_c range from ~10^{-3} to ~10^{-2} for rocks and many other polycrystalline brittle solids. This criterion can simulate both tensile-induced and shear-induced rock failures.

In combination with the DEM network, we use a collection of conjugate flow node to explicitly calculate the pressure change caused by injection. The governing equation for fluid flow is

$$\frac{\partial\left(\phi\rho_f\right)}{\partial t} = \nabla\left(\frac{\rho_f k}{\mu}\nabla P\right) + Q \qquad (7)$$

where ϕ is the porosity of porous medium, ρ_f is the density of injected fluid, k is the formation permeability, μ is the fluid viscosity, P is the pressure, and Q is the injection rate. Fluid pressure at each conjugate flow node is updated during every time step. The more detailed descriptions about fluid flow and coupling process can be found in Zhou 2016[22]. These pressure changes will exert additional forces on the neighboring DEM particles as equivalent body forces.

Therefore, the total force and moment of each DEM particle is obtained after considering the force exerted due to the fluid pressure gradient.

$$\vec{F}_{i,j} = k_n\left(d_{i,j} - d_{i,j}^0\right)\vec{n}_{i,j} + k_s\frac{1}{2}\left(\phi_{i,j} + \phi_{j,i}\right)\vec{s}_{i,j} - \nabla P\cdot\pi r_i^2 \quad (8)$$

$$\overrightarrow{M}_{i,j} = k_s d_{i,j}\left[\frac{\Phi}{12}\left(\phi_{i,j} - \phi_{j,i}\right) + \frac{1}{2}\left(\frac{2}{3}\phi_{i,j} + \frac{1}{3}\phi_{j,i}\right)\right] \quad (9)$$

∇P is the fluid pressure gradient acting on individual DEM particle, obtained from the nodal pressure values on its neighboring conjugate flow lattice. As fluid pressure (and pressure gradient) increase due to fluid injection during hydraulic stimulation, the force exerted on the DEM particles also increases and deforms the mechanical bonds and breaks them if the deformation reaches the prescribed threshold value, thereby initiating fracturing. The beam moment is not affected by the pressure gradient. When a mechanical bond is broken, a microfracture perpendicular to the bond is initiated and connects the two associated fluid nodes of the flow network with a new permeability in the form

$$k = \frac{b^2}{12} \qquad (10)$$

here b is the aperture of the microfracture, which is the same as the separation distance of the two neighboring DEM particles subject to fracturing.

3. MODEL VALIDATION

In order to validate our numerical model in predicting the hydraulic fracture propagation, we compare our model with the typical analytical solutions of KGD and PKN model. The detailed equations of these two models are summarized in Table 1. In these models, i is the half of injection rate, h is fracture height, μ is the injection viscosity, t is the total injection time. We adopt the same parameters used in Kan Wu 2014 [15]. Since the model is still two dimensional, we assume that the generate fracture has a constant height in the z direction, which equals to 60.96 m (200 *ft*). The comparison of fracture half-length and maximum width between KGP, PKN and proposed DEM model are shown in figure 4 and 5.

Table 1. Analytical solutions of KGD and PKN

	Fracture Half Length	Maximum Fracture Width
KGD	$0.539\left(\frac{i^3E'}{\mu h^3}\right)^{1/6} t^{2/3}$	$2.36\left(\frac{\mu i^3}{E'h^3}\right)^{1/6} t^{1/3}$
PKN	$0.524\left(\frac{i^3E'}{\mu h^4}\right)^{1/5} t^{4/5}$	$3.04\left(\frac{\mu i^2}{E'h}\right)^{1/5} t^{1/5}$

Table 2. The input parameters for model validation

Input parameters	
Injection Viscosity μ	100 cP
Injection Rate	20 bpm
Young's Modulus	6,530,000 psi
Poisson's Ratio	0.2
Height	200 ft
Minimum Horizontal Stress	4450 psi

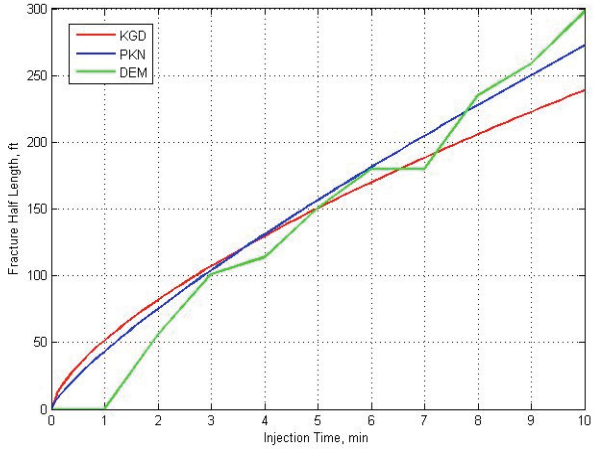

Fig. 4. The fracture half-length versus injection time from KGD, PKN and DEM model.

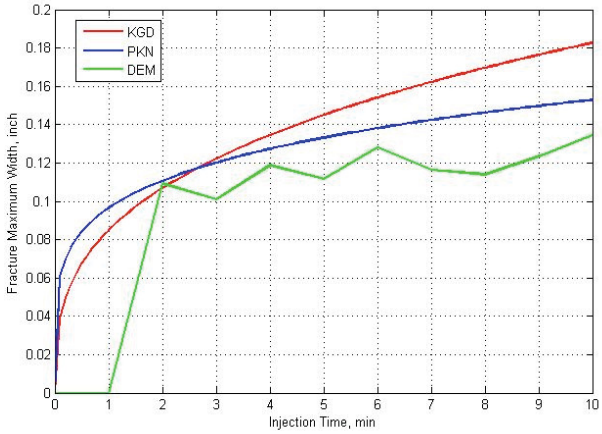

Fig. 5. The fracture maximum width versus injection time from KGD, PKN and DEM model.

Both the fracture half-length and fracture width obtained from our DL-DEM simulator exhibit a good match with KGD and PKN model. However, at the initial injection time ($t < 2$ min), our model requires a longer time to accumulate the pressure in the wellbore to break a bond and form micro fractures. Therefore, when the injection time is less than 1 min, there is no fracture generated. The same phenomenon can be observed in the fracture width plot. Moreover, since the DEM utilizes bond breakage to mimic the fracture propagation, it is a discontinuous method. Microstructure randomness is introduced to the algorithm through the random placement of particles. Thus the fracture will display different propagation speed at different times. The width fluctuation is also caused by the particle interactions and movements.

4. NUMERICAL RESULTS

4.1. Rock Heterogeneity in the Micro/Meso Scale

The nature of rock mass is discontinuous, anisotropic and inhomogeneous. The DL-DEM method is a mesh-free discontinuous method described by discretizing the whole domain into an assembly of particles. The heterogeneity can be directly incorporated in the algorithm through the assignment of different properties to particles. In this section, we are going to investigate the impact of rock heterogeneity under micro/meso scale.

Figure 6 represents a small piece of rock sample. In this rock sample, there are five irregular shape grains (green area) with properties different from the main rock formation (red formation). In order to describe both intra-grain and inter-grain heterogeneity, two different scenarios are considered here: (1) weaker interfaces exist between the grains and rock formations (Figure 6 (a) dark blue lines) (2) the grains are directly in contact with rock formation without any interface (Figure 6(b)). It is assumed that the heterogeneous grain is much weaker than the rock formation (smaller critical strain). The deformations of the both rock samples under uniaxial compressive stress are shown in figure 7.

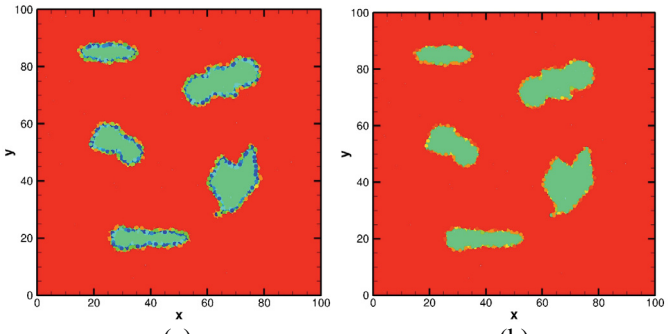

(a) (b)

Fig. 6. The schematic of two different rock sample heterogeneities.

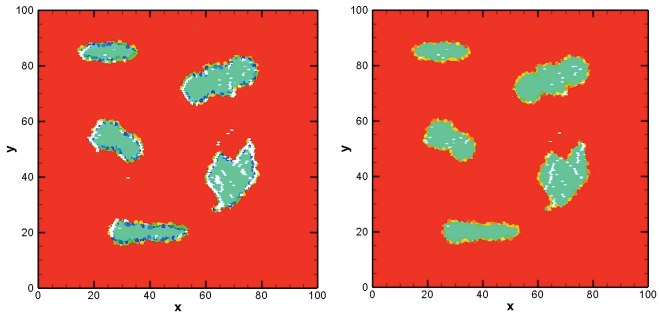

(a) (b)

Fig. 7. The deformation of the rock sample under uniaxial compressive stress.

After applying the same amount of compressive stress on the rock sample, for the first scenario, the generated cracks are mainly focused on the weaker interface. But if no weaker boundary exists, the micro crack will be generated in the middle of the heterogeneous rock grains. The weaker the interface, the easier to induce the microcracks under uniaxial compressive stress.

4.2. Field Case Heterogeneity

For the sedimentary basin, many reservoirs will be complex, layered, and not homogeneous. Rock properties and hydraulic parameters such as Young's modulus, strength, permeability, and porosity can vary strongly in space due to the movements of the upper crust of the Earth, including tectonic movements, earthquakes, land lifting/subsidence, glaciation cycles, and tides [23], [24]. These heterogeneities of reservoir formation will significantly impact the hydraulic fracturing.

After examining the small-scale case, we are going to apply our method to a realistic unconventional reservoir to demonstrate the capability of our simulator in real industry application. The detailed reservoir properties can be obtained based on the well log information. In order to investigate the impact of rock heterogeneity on hydraulic fracture propagation, three models are used in this section:

1. Homogeneous reservoir
2. Coarse model with 5 layers
3. High resolution model with 24 layers

We assume that each layer is homogeneous and shares the same properties, including permeability, porosity, Young's modulus, and unconfined compressive strength. In all models, the layers' properties are obtained through averaging the information according to their depths. Inevitably, the coarser the model, the more information will be lost during the averaging process.

4.2.1. Homogeneous Reservoir Model

Based on the detailed well-log information, the homogeneous model is obtained through averaging the whole pay zone properties including Young's modulus, permeability, etc. In this example, we simulate a single stage of a reservoir with the size of 106.68 m (350 *ft*) × 60.96 m (200 *ft*) (*xz* plane). A horizontal wellbore is located at z = 43.28 m *(142 ft)* with five perforation clusters. The spacing between the perforation clusters is 21.34 m (70 *ft*). Five point sources are used to represent the five clusters. The averaged Young's modulus is 6.2 *MMpsi* and the averaged permeability is 0.1868 *md*. The stress difference is 1000 *psi* with the maximum stress direction oriented in the z direction. Due to the absence of stress gradient, the hydraulic fractures will grow upward and downward simultaneously after the injection starts. Figure 8 and 9 give the induced hydraulic fracture pattern and net pressure distribution in this homogenized reservoir.

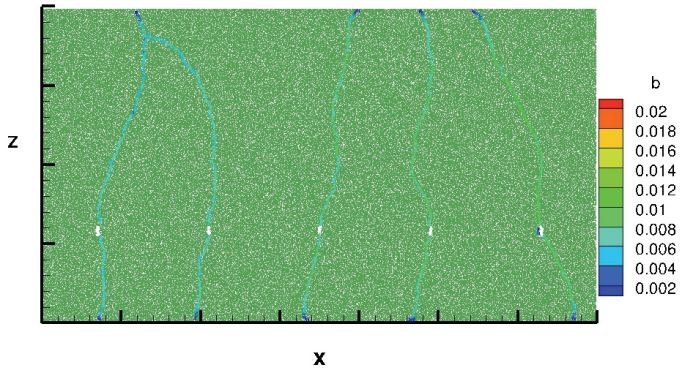

Fig. 8. Hydraulic fracture pattern of the homogeneous reservoir.

As the fluid is injected, the pressure at the five perforations begins to build. Once the pressure at certain perforation is large enough to break the bond of particles, fracture will initialize and start to propagate. Without any rock heterogeneity, the fractures will propagate continuously toward the boundary. There is no significant fracture aperture or direction change during propagation. But the crack opening in one perforation will cause additional compressive stress accumulation in the neighborhood, which may reorient the nearby local principal stress direction and alter the fracture propagation direction.

In figure 9, the blue zone around the induced hydraulic fracture represents the fluid leakoff from the fracture to formation. The area of this blue zone is directly related to the formation permeability. Since it is a homogeneous reservoir, the whole domain shares single permeability. The leakoff affected zones of the five induced fractures are almost the same.

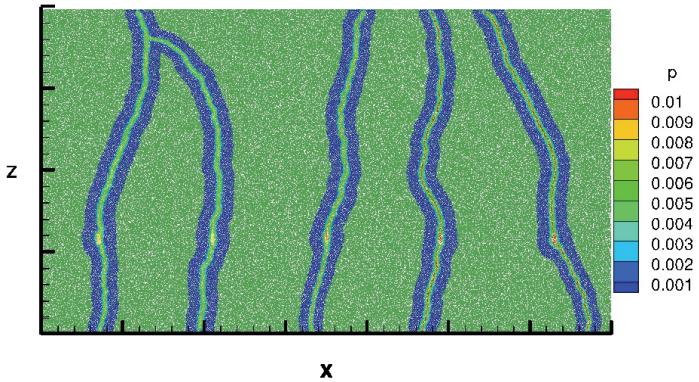

Fig. 9. Dimensionless net pressure (the ratio of net pressure to Young's modulus) distribution of the homogeneous reservoir.

4.2.2. Coarse Heterogeneous Model with 5 Layers

Figure 10 describes a side-view (*xz* plane) of the reservoir domain without considering the stress gradient in the z direction. The whole domain is separated into 5 layers with different properties, which are clearly marked in the picture. The horizontal wellbore is shown as the red lines.

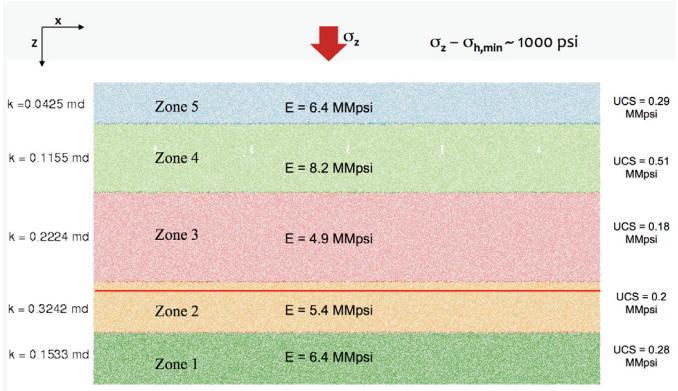

Fig. 10. Reservoir domain and parameters used in the coarse model with 5 layers.

Figure 11 depicts the induced hydraulic fracture geometry, which clearly shows that the fractures propagate smoothly until they reach zone 4. Zone 4 has a large Young's modulus and unconfined compressive strength (UCS), therefore the rock at this layer is hard to break and able to absorb more energy, which in turn, impedes the propagation. Moreover, due to the large perforation spacing and large stress difference, the generated fractures tend to grow without large interference.

The color of generated fractures explicitly represents the fractures' aperture. It is obvious that all fractures are non-uniform and the aperture varies according to layer's properties. Among all the 5 zones, zone 3 has the largest aperture. On the contrary, the subsection of the fracture in zone 4 exhibits the smallest aperture, which is due to the large Young's modulus and the difficulty of breaking the rock.

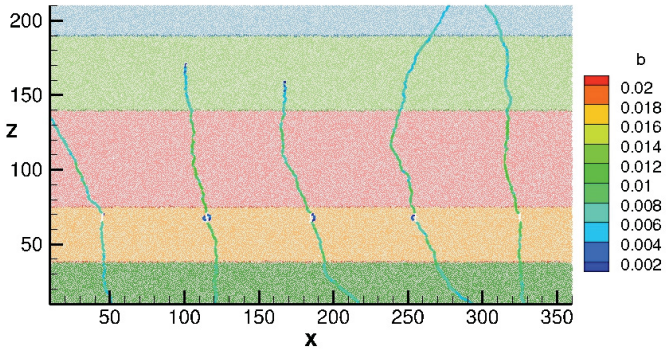

Fig. 11. Hydraulic fracture pattern in the coarse heterogeneous model with 5 layers.

Figure 12 gives the pressure distribution after hydraulic fracture propagation. The amount of fluid leakoff is determined by both rock properties and permeability. It can be seen that zone 1 ~ 3 have similar, relatively high permeability, which leads to more fluid flow from fracture to formation. On the contrary, zone 5 has a relatively low permeability (k = 0.0425 *md*), so the blue zone which represents leakoff area is very small.

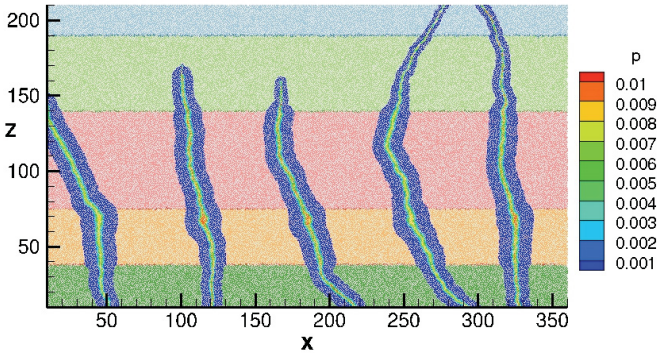

Fig. 12. Dimensionless net pressure (the ratio of net pressure to Young's modulus) distribution in the coarse heterogeneous model with 5 layers.

4.2.3. High Resolution Model with 24 Layers

The same reservoir but under higher resolution is then used as a comparison case to further explain the impact of formation heterogeneity on fracture pattern, the side view (*xz* plane) of which is shown in Figure 13. The stress gradient in *z* direction is also not included in this section.

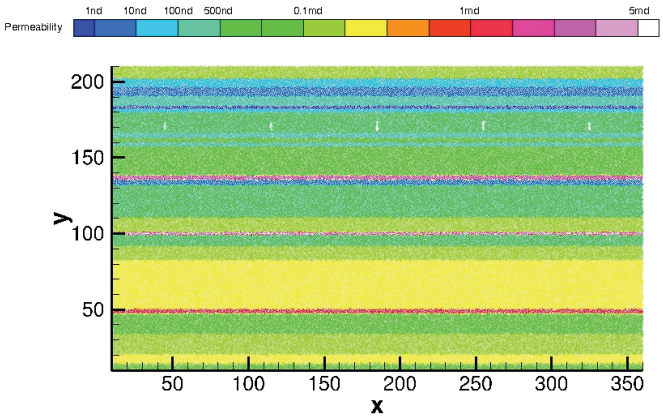

Fig. 13. Reservoir domain of the high resolution model with 24 layers.

Comparing the 24-layers model (Figure 13) with the 5-layers model (Figure 10), it is obvious that under high resolutions, the reservoir contains three thin layers of high-permeability zone in the middle of the domain (on the order of millidarcy, represented as the red color) and three layers with extremely low permeability at the top of the domain (at the order of nanodarcy, represented as the deep blue color). However, those distinct heterogeneous properties disappear in the coarse model because of the averaging process. In the 5-layer model, the property contrast between layers is not significant. Therefore the fracture will propagate along the in-situ stress direction and remain bi-wing in geometry in the coarse model (Figure 11).

In order to avoid the other possible disturbances brought to the fracture propagation, well location, number of

perforations, injection rate and viscosity in this high-resolution model remain the same as in the previous example. The induced hydraulic fractures are shown in Figure 14.

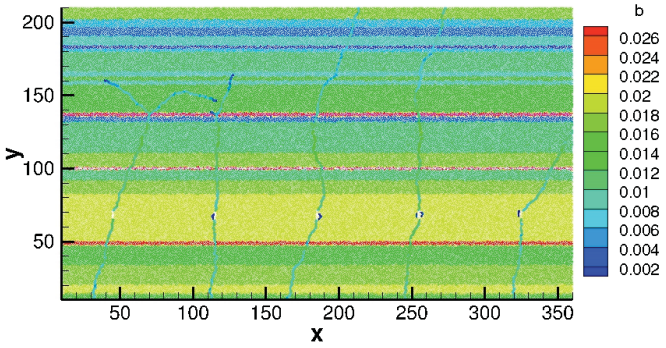

Fig. 14. Hydraulic fracture pattern of the 24 layers heterogeneous reservoir.

First of all, the generated fracture conductivity has also a non-uniform distribution, and the apertures reflect the Young's modulus and critical tensile/shear strain. Without considering the stress gradient in the depth direction, the fracture will propagate in both directions (up and down) simultaneously after injection.

Most of the induced hydraulic fractures (4 out of 5) maintain their bi-wing geometry parallel to the far field maximum stress direction. But one of the fractures branches at the high-permeability zone interface. Instead of growing with the original propagation direction, the branched fracture actually alters its direction and propagates along the interface.

Figure 15 depicts the pressure distribution after hydraulic fracture propagation. Compared with the coarse model (Figure 12), the net pressure distribution is more complex and directly reflects the layer's permeability. In the high-permeability zone, the injection fluid will largely leak into the layer and increase the zone pressure. Large amount of fluid leakoff means that the effective injection rate used to drive the fracture open will be correspondingly decreased. This reduction of effective injection rate is one of the primary reasons leading to fracture branch at the interface.

Therefore, ignoring the formation heterogeneity or simplifying the model with property averaging technique may lead to biased fracture predictions.

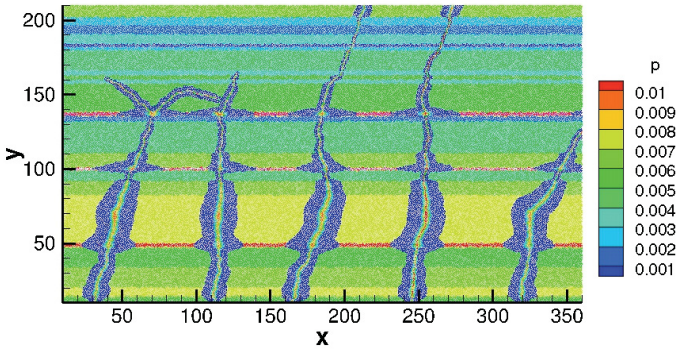

Fig. 15. Dimensionless net pressure (the ratio of net pressure to Young's modulus) distribution of the 24 layers heterogeneous reservoir.

5. CONCLUSIONS

In this paper, the proposed dual-lattice DEM simulator has been applied to both a rock sample and a realistic field reservoir with different layer resolutions. From the simulation results, we can conclude that the formation's heterogeneity will impact the induced hydraulic fracture pattern, especially when the layer permeability and mechanical properties contrast are large. Both high permeability and large critical tensile/shear strain will reduce the fracture propagation velocity and distance. Larger Young's modulus indicates that the rock is harder to move, which in turn leads to smaller fracture aperture. Moreover, the differences of rock properties may lead to fracture branching and alter the fracture propagation direction. As a result, ignoring significant layer contrast in fracture simulation will lead to a biased fracture prediction. Therefore, the conventional simulator with homogeneous assumption is not applicable for highly heterogeneous shale formation.

REFERENCES

[1] P. Valkó and M. J. Economides, *Hydraulic Fracture Mechanics*. WILEY, 1996.

[2] E. L. Hagström and J. M. Adams, "Hydraulic Fracturing: Identifying and Managing the Risks," *Environ. Claims J.*, vol. 24, no. 2, pp. 93–115, 2012.

[3] T. H. Yang, L. G. Tham, C. A. Tang, Z. Z. Liang, and Y. Tsui, "Influence of Heterogeneity of Mechanical Properties on Hydraulic Fracturing in Permeable Rocks," *Rock Mech. Rock Eng.*, vol. 37, no. 4, pp. 251–275, 2004.

[4] J. Zhou, H. Huang, and M. Deo, "Modeling the Interaction Between Hydraulic and Natural Fractures Using Dual-Lattice Discrete Element Method," in *49th US Rock Mechanics / Geomechanics Symposium held in San Francisco, CA, USA, 28 June- 1 July*, 2015.

[5] J. McLennan, D. Tran, N. Zhao, S. Thakur, M. Deo, I. Gil, and B. Damjanac, "Modeling Fluid Invasion and

Hydraulic Fracture Propagation in Naturally Fractured Rock : A Three-Dimensional Approach," in *2010 SPE International Symposium and Exhibition on Formation Damage Control, Lafayette, Louisiana, USA, 10-12 February.*, 2010, pp. 1–13.

[6] J. Adachi, E. Siebrits, A. Peirce, and J. Desroches, "Computer simulation of hydraulic fractures," *Int. J. Rock Mech. Miniing Sci.*, vol. 44, pp. 739–757, 2007.

[7] Q. Li, H. Xing, J. Liu, and X. Liu, "Review article A review on hydraulic fracturing of unconventional reservoir," *Petroleum*, vol. 1, pp. 8–15, 2015.

[8] S. A. Khristianovic and Y. P. Zheltov, "Formation of Vertical Fractures by means of Highly Viscous Liquid," in *4th World Petroleum Congress*, 1955, vol. 5.

[9] J. Geertsma and F. d. Klerk, "A Rapid Method of Predicting Width and Extent of Hydraulically Induced Fractures," *J. Pet. Technol.*, vol. 21, no. 12, pp. 1571–1581, 1969.

[10] T. K. Perkins and L. R. Kern, "Widths of Hydraulic Fractures," *J. Pet. Technol.*, vol. 13, no. 09, pp. 937–949, Apr. 1961.

[11] R. P. Nordgren, "Propagation of a Vertical Hydraulic Fracture," *Soc. Pet. Eng. J.*, vol. 12, no. 04, pp. 306–314, 1972.

[12] N. Zhao, J. McLennan, and M. Deo, "Morphology and Growth of Fractures in Unconventional Reservoirs," in *Canadian Unconventional Resources Conference,15-17 November, Calgary*, 2011, pp. 1–14.

[13] J. Huang, C. Yang, X. Xue, and A. Datta-Gupta, "Simulation of Coupled Fracture Propagation and Well Performance under Different Refracturing Designs in Shale Reservoirs," in *SPE Low Permeability Symposium, Denver, Colorado, USA, 5-6 May,* 2016.

[14] S. L. Crouch, "Solution of plane elasticity problems by the displacement discontinuity method," *Int. J. Numer. Methods Eng.*, vol. 10, no. 2, 1976.

[15] K. Wu, "Numerical Modeling of Complex Hydraulic Fracture Development in Unconventional Reservoirs,"Ph.D. Thesis, the University of Texas at Austin, 2014.

[16] D. H. Shin and M. M. Sharma, "Factors Controlling the Simultaneous Propagation of Multiple Competing Fractures in a Horizontal Well," in *SPE 168599 Hydraulic Fracturing Technology Conference, Woodlands, Texas, USA, 4-6 February*, 2014, no. 2009.

[17] N. Moës, J. Dolbow, and T. Belytschko, "A Finite Element Method for Crack Growth Without Remeshing," *Int. J. Numer. Methods Eng.*, vol. 46, no. 1, pp. 131–150, 1999.

[18] J. Zhou, H. Huang, and M. Deo, "A New Physics-Based Modeling of Multiple Non-Planar Hydraulic Fractures Propagation," in *URTeC 2170875. Unconventional Resources Technology Conference held in San Antonio, Texas, USA, 20-22 July*, 2015.

[19] F. Zhang, B. Damjanac, and H. Huang, "Coupled discrete element modeling of fluid injection into dense granular media," *J. Geophys. Res. Solid Earth*, vol. 118, no. 6, pp. 2703–2722, 2013.

[20] D. O. Potyondy and P. a. Cundall, "A bonded-particle model for rock," *Int. J. Rock Mech. Min. Sci.*, vol. 41, no. 8, pp. 1329–1364, Dec. 2004.

[21] H. Huang and E. Mattson, "Physics-based Modeling of Hydraulic Fracture Propagation And Permeability Evolution of Fracture Network In Shale Gas Formation," in *2014 ARMA 48th US Rock Mechanics/Geomechanics Symposium,Minneapolis, MN, 1-4 June 2014*, 2014.

[22] J. Zhou, "Hydraulic Fracture Propagation Modeling and Data-based Fracture Identification," Ph.D. Thesis, Department of Chemical Engineering, the University of Utah, 2016.

[23] L. Jing, "A review of techniques, advances and outstanding issues in numerical modelling for rock mechanics and rock engineering," *Int. J. Rock Mech. Min. Sci.*, vol. 40, no. 3, pp. 283–353, 2003.

[24] A. Kissinger, R. Helmig, A. Ebigbo, H. Class, T. Lange, M. Sauter, M. Heitfeld, J. Klünker, and W. Jahnke, "Hydraulic fracturing in unconventional gas reservoirs : risks in the geological system , part 2," *Environ. Earth Sci.*, vol. 70, no. 8, pp. 3855–3873, 2013.